THE ASTROPHYSICAL JOURNAL, 278:369–381, 1984 March 1

SELF-CONSISTENT MODELS FOR COULOMB-HEATED X-RAY PULSAR ATMOSPHERES

A. K. HARDING
NASA Goddard Space Flight Center, Laboratory for High Energy Astrophysics
P. MÉSZÁROS[1]
Harvard-Smithsonian Center for Astrophysics
AND
J. G. KIRK AND D. J. GALLOWAY
Max-Planck-Institut für Physik und Astrophysik MPA
Received 1983 February 10; accepted 1983 August 16

ABSTRACT

We present detailed calculations of accreting magnetized neutron star atmospheres heated by the gradual deceleration of protons via Coulomb collisions. Self-consistent determinations of the temperature and density structure for different accretion rates are made by assuming hydrostatic equilibrium and energy balance, coupled to radiative transfer. The full radiative transfer in two polarizations, using magnetic cross sections but with cyclotron resonance effects treated approximately, is carried out in the inhomogeneous atmospheres. For $\dot{M} \lesssim 10^{17}$ g s^{-1}, the equilibrium atmospheres have temperatures and optical depths which are very sensitive to the strength of the surface magnetic field. Because of a decreased efficiency of cyclotron line cooling, atmospheres with higher magnetic fields are hotter, more optically thin, and radiate harder spectra. The computed pencil beam pulse shapes show frequency-dependent structure: for a wide range of aspect angles, the pulses switch from single to multiple below $\sim\omega_H/4$, and there is a general hardening of the spectral index toward midpulse.

Subject headings: polarization — pulsars — radiative transfer — stars: accretion — stars: neutron

I. INTRODUCTION

An outstanding problem in the theory of accreting magnetized neutron stars is the lack of a unique, self-consistent model of the accretion column, resulting in major uncertainties about how the spectrum and the pulses are produced. Given that many of our determinations of neutron star masses, radii, and magnetic field strengths have come from such accreting systems, it is vital to understand in more detail the origin of the radiation from which all this information is gleaned. It is known that for high luminosities, $L_X \gtrsim 10^{37}$ ergs s^{-1}, radiation pressure plays a major role in decelerating the accreting matter (Basko and Sunyaev 1976; Wang and Frank 1981). However, for luminosities $L_X \lesssim 10^{37}$ ergs s^{-1}, to which we shall confine ourselves, it is not clear whether the deceleration occurs gradually via Coulomb encounters, through inelastic nuclear collisions, or by the formation of a collisionless shock (Zel'dovich and Shakura 1969; Lamb, Pethick, and Pines 1973; Langer and Rappaport 1982). This question is still unsettled, and because of this basic uncertainty the best approach at present is to investigate the observational consequences predicted by different models, in the hope of thus being able to distinguish among them.

In the present paper we study the gradual deceleration model and argue that in most cases Coulomb collisions will be more effective than nuclear collisions. We calculate the temperature and density gradients in hydrostatic and energy equilibrium, coupled to the fully magnetized radiative transfer including vacuum polarization effects. Preliminary results of this calculation have been presented in Mészáros *et al.* (1983). We include the effects of cyclotron line cooling in an approximate way, but we do not attempt to predict the details of the line spectrum, since a full theory for the transfer near the resonance is still missing (Wasserman and Salpeter 1980; Bussard 1980; Kirk and Mészáros 1980; Nagel 1980). We find that such Coulomb-heated atmospheres are rather shallow, of height $z \lesssim 10^3$ cm, which is much less than the radius of the emitting polar cap. Previous calculations of the spectrum for such plane-parallel atmospheres with $\boldsymbol{B}$ parallel to z have previously been made assuming a homogeneous slab or semi-infinite medium, with an estimated density and temperature (Bonazzola, Heyvaerts, and Puget 1979; Ventura, Nagel, and Mészáros 1979; Mészáros, Nagel, and Ventura 1980; Nagel 1980). Here we calculate the continuum spectrum from the self-consistent density and temperature stratification of the medium. We have not included the possible effect of absorption by matter farther away than the immediate vicinity of the polar cap regions (McCray and Lamb 1976; Basko and Sunyaev 1976), nor the possible effects of interstellar absorption, which may cause a low-energy turnover. Incoherent scattering is implicit in our treatment of the line transfer, and Compton cooling is included in the energy balance and in the atmospheric structure calculation. However, the continuum spectrum is calculated assuming coherent scattering. Introducing incoherent scattering should not change the continuum spectrum very much for our range of $\dot{M}$, but an accurate prediction of observable cyclotron line profiles would require a more elaborate treatment.

We have also calculated the intrinsic beaming pattern of the radiation escaping from the stratified atmosphere. Previous calculations of beam patterns for plane-parallel atmospheres with $\boldsymbol{B}$ perpendicular to the surface assumed an estimated homogeneous density and temperature (Tsuruta 1975; Basko

[1] Smithsonian Visiting Scientist, on leave from Max-Planck-Institut für Physik und Astrophysik MPA, Garching, West Germany.

and Sunyaev 1975; Nagel 1981*a*; Mészáros and Bonazzola 1981). Calculations of beam patterns from atmospheres with cylindrical geometry (Yahel 1980; Nagel 1981*a*; Pravdo and Bussard 1981) have also assumed a homogeneous density and temperature, or taken an estimated distribution. The beam patterns found in the present work, arising from the self-consistent inhomogeneous (plane parallel) atmospheres heated by Coulomb deceleration, are of the pencil beam type. They are characterized at many aspect angles by single pulses at high frequencies which break up into multiple pulses at lower frequencies. The breakup frequency, within some limitations, corresponds to a submultiple of the cyclotron frequency, and this can give an indirect estimate of the field strength. We also discuss the phase dependence of the spectrum, in terms of spectral index versus phase plots. The present models show a general, but not universal, tendency for the spectrum to change most rapidly toward midpulse. The details of both the pulse shape and the spectral index versus phase behavior are dependent on the magnetic field strength and the viewing angle, as well as on the specific temperature and density gradients in the atmosphere.

In the final section of the paper we discuss some of the implications of these calculations and compare them with other models and with available observations.

II. PHYSICAL PROCESSES IN STRONG MAGNETIC FIELDS

There are several major complications which arise in the presence of a strong magnetic field due to the quantization of electron energy perpendicular to the field. First, the radiation propagates in two normal polarization modes, each with rather different opacities, which are coupled by polarization exchange scattering. Second, the proton stopping is somewhat more complicated, as the strong field will partially inhibit the exchange of momentum with the atmospheric electrons. The equations are of a similar character to the nonmagnetic case as treated by Zel'dovich and Shakura (1969) and Alme and Wilson (1973), but a detailed treatment of the magnetic peculiarities makes it necessary to resort to a numerical calculation.

We assume a plane-parallel atmosphere, varying only along the z-coordinate perpendicular to the surface (i.e., parallel to the field $\boldsymbol{B}$). The grammage traversed by a proton falling into the atmosphere is defined by

$$y = \int_z^\infty \rho(z) dz \tag{1}$$

in units of g cm^{-2}. The plane-parallel atmosphere is assumed to extend laterally over an area $A = \pi R_p^2$, where R_p is the magnetic polar cap radius, there being one such area at each pole. For a certain magnetic field strength and accretion rate, we determine the polar cap radius R_p as a function of the Alfvén radius. For an Alfvén surface interacting with an accretion disk, we use a formula originally due to Lamb, Pethick, and Pines (1973) for the Alfvén radius, which we rewrite as

$$R_A(\text{disk}) = 3 \times 10^7 \alpha^{18/69} \dot{m}^{-16/69} m^{-13/69} R_6^{120/69} B_{12}^{40/69} \text{ cm} . \tag{2}$$

We have used the disk parameters of Shakura and Sunyaev (1973), case (b), where $\sigma_T > \sigma_{ff}$, $\rho^{gas} > \rho^{rad}$, and $\alpha \leq 1$ is the viscosity parameter, $m = M/M_\odot$, $\dot{m} = \dot{M}/1.3 \times 10^{18} m$, $R_6 = R_N/10^6$ cm, $B_{12} = B/10^{12}$ G. In terms of R_A and R_N, the polar cap radius is $(R_p/R_N)^2 \approx R_N/R_A$, so that

$$(R_p/R_N) \approx 0.16 \alpha^{-9/69} \dot{m}^{8/69} m^{13/138} R_6^{-51/138} B_{12}^{-20/69} . \tag{3}$$

Thus, for $B = 4.4 \times 10^{12}$ G, and $\dot{M} = 10^{17}$, 10^{16}, 10^{15}, and 10^{14} g s^{-1}, $m = \alpha = 1$, $R_6 = 1.2$, we get, respectively, $R_p = 8.83$, 6.66, 5.0, and 4.6×10^4 cm.

a) Deceleration of the Accretion Flow

The interaction between the accreting material and the atmosphere was treated using the techniques described by Kirk and Galloway (1981, 1982), in which the effect of small-angle Coulomb scattering is considered. Early work in this field (Basko and Sunyaev 1975; Pavlov and Yakovlev 1976) had indicated that such small-angle scattering processes were inhibited by the strong magnetic field in a neutron star's atmosphere. In this case nuclear collisions between accreting protons and protons of the atmosphere would become important and limit the penetration depth to about 50 g cm^{-2}. However, these calculations assumed that the accreting protons move on a rectilinear path through a cold electron gas. They are no longer valid when the thermal velocity of electrons in the atmosphere ceases to be negligible compared with the speed of the accreting particles, and when the gyroradius of the proton is of the same order of magnitude as the Debye screening length. Under such circumstances, the effect of small-angle Coulomb collisions between accreting protons and electrons of the atmosphere is, in fact, enhanced, and the upper limit to the penetration depth provided by nuclear collisions is not always relevant.[2] As in the zero magnetic field case (Sitenko 1967), proton-proton Coulomb collisions are unimportant in the deceleration problem.

The method of Kirk and Galloway consists of calculating the dynamic friction and diffusion coefficients for a heavy, charged test-proton moving in a strongly magnetized, homogeneous electron gas of specified temperature and density. The main assumptions involved in this procedure are that the electron gas responds linearly to the presence of the test particle, and that its state is well approximated by a gas in which only the lowest Landau level is populated (Kirk 1980). These conditions are fulfilled in the case of accretion onto a neutron star provided that the density of the atmosphere exceeds that of the accretion flow, and that the energy density in radiation at the cyclotron resonance frequency is not too large. The latter requirement arises because collisional processes are ineffective at exciting electrons into higher Landau levels at densities less than 10^{26} cm^{-3}. As a result, the population of these levels is controlled by the radiation field and is not directly related to the dispersion of electron velocity along the field lines. Thus, even a plasma at a temperature of 10^9 K will contain electrons in only the lowest Landau level, provided that the number density of photons at the resonant frequency ω_H is much smaller than the corresponding blackbody density at a temperature $T = \hbar\omega_H/k$. The coefficients thus calculated are inserted into the Fokker-Planck equation, which can then be solved to give the evolution in time of a specified distribution of test particles. The interactions

[2] As an example, a proton of initial speed $c/2$ is stopped in a uniform plasma of $n_e = 10^{23}$ cm^{-3}, $T_e = 20$ keV, $B = 5 \times 10^{12}$ gauss in a length of $y_0 = 20$ g cm^{-2}.

of test particles with each other are neglected. The initial distribution is chosen to describe protons moving rapidly along the magnetic field lines in a homogeneous plasma. The initial distribution function assumed for this calculation is a Maxwellian at temperature $T_i = 500$ keV centered on $v_\perp = 0$, $v_\parallel = c/2$. Averages over the distribution at subsequent times then give the energy and momentum which are delivered by the accreting protons to the plasma of the atmosphere during the various stages of deceleration.

In order to adapt this method to the inhomogeneous atmosphere of a neutron star, a three-dimensional table was established in electron density, electron temperature, and proton kinetic energy. At each point the rate of loss of momentum $d\Pi/dy$ and energy dE/dy of the accretion flow was evaluated from one of the solutions of the Fokker-Planck equation, enabling interpolation over the range $n_e = 10^{16}$–10^{25} cm^{-3}, $T_e = 5$–90 keV, and proton kinetic energy $E =$ 120–5 MeV. The dependence on B is very weak compared with the dependence on n_e and T, since B appears only in the Coulomb logarithm (see Langer and Rappaport 1982, eq. [C4]). The neglect of the magnetic field strength dependence of the loss rates therefore does not introduce much error. Figure 1 shows the proton energy loss rates calculated in this way for $n_e = 10^{23}$ cm^{-3} with the corresponding nonmagnetic loss rates (cf. Alme and Wilson 1973) also shown for comparison.[3]

In such an interpretation it is implicitly assumed that the interaction between accreting electrons and atmospheric electrons proceeds relatively quickly. Charge neutrality is preserved by the establishment of a small return current in the atmosphere, in a manner similar to that in the X-ray producing regions associated with solar flares (Emslie 1980). Although it cannot be ruled out that a collisionless shock front will establish itself where the accreting matter meets the atmosphere (Langer and Rappaport 1982), this nevertheless seems unlikely, in view of the stabilizing influence of the magnetic field and the inefficiency of electrostatic instabilities (McKee 1970; Alme and Wilson 1973; Kirk and Trümper 1982).

[3] The energy and momentum loss rates used in this paper are a factor of 2 smaller than those presented by Kirk and Galloway (1981, 1982), thus canceling an error of this factor which was present in their original calculations.

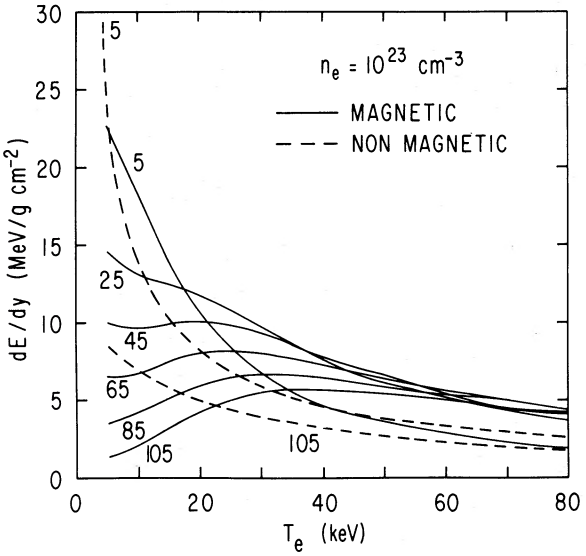

FIG. 1.—Proton energy loss rate as a function of atmospheric electron temperature for different mean proton energies in MeV.

In addition, we also include the effects of stopping by nuclear collisions, for which the energy loss rate is taken to be

$$\left(\frac{dE}{dy}\right)_N = \frac{E}{y_N} e^{-y/y_N}$$

(Basko and Sunyaev 1975), where the total stopping length $y_N = 50$ g cm^{-2}. This deceleration rate and the corresponding momentum loss rate, taking $p = (2mE)^{1/2}$, are added to the Coulomb loss rates, since nuclear scattering is an independent process.

b) Radiative Cooling

We include three contributions to the cooling of the atmosphere: bremsstrahlung emission Λ_B, Compton scattering Λ_C, and collisional excitation of electrons to the first excited Landau state followed by the emission of cyclotron line photons, Λ_L. We thus write the total cooling rate as

$$\Lambda = \Lambda_B + \Lambda_C + \Lambda_L . \quad (4)$$

The inverse bremsstrahlung (absorption) and Compton (photon energy loss to electrons) processes result in heating of the atmosphere and are therefore included in the net cooling rate. The inverse of Λ_L, absorption of a line photon followed by collisional de-excitation, should be a negligible contribution. Since the radiative de-excitation rate is much larger, line photons are expected to escape into the adjacent continuum by nonresonant scatterings before they are absorbed.

A correct treatment of the line transfer is extremely time-consuming when computing an inhomogeneous atmosphere by iterations, as is done below, so that some approximation is called for. The scattering cross section is resonant, which would increase the inverse Compton cooling rate, but on the other hand, photons should be scattered out of the line fairly quickly, so that most of the scattering should occur in the continuum. The theory of resonant line transfer is extremely complicated (Wasserman and Salpeter 1980; Kirk and Mészáros 1980; Nagel 1981*b*; Bussard and Lamb 1982) and not yet fully understood.

The contribution of the cyclotron resonance to the cooling is therefore treated in an approximate way by including a term for the production rate of line photons which is proportional to the rate of collisional excitations. Using the combined rates of electron-electron and electron-ion collisions from Langer and Rappaport (1982), we write the cyclotron line emissivity as

$$\Lambda_L \approx 1.22 \times 10^{-20} P_{esc} B_{12}^{-1/2} n_e^2 \left[1.50 + 3.73 \left(\frac{kT}{\hbar\omega_H}\right)^{1/2}\right] \times \exp\left\{\frac{-m_e c^2}{kT}\left[(1 + 0.04531 B_{12})^{1/2} - 1\right]\right\} \text{ ergs cm}^{-3}\text{ s}^{-1} , \quad (5)$$

where P_{esc} is the probability that the line photons leave the resonance before being absorbed. These photons are thus assumed to appear with probability P_{esc} in the line wings, where they scatter as continuum photons. As argued by Langer and Rappaport (1982), P_{esc} is very near 1 for the expected densities and temperatures; i.e., a line photon will typically suffer a

nonresonant scattering into the wings of the resonance before it can undergo enough resonant scatterings to have a significant probability of suffering a true absorption (radiative excitation followed by collisional de-excitation). Therefore, we take $P_{esc} = 1$ in almost all cases, although we have considered a few cases where $P_{esc} = 0.1$. Actually, a value of $P_{esc} < 1$ can also mimic the effect of a departure of the electron distribution from a pure Maxwellian. Langer, McCray, and Baan (1980) find that departures from a Maxwellian distribution result in lower line emissivity. The above emissivity is divided equally between two adjacent frequency bins, $\omega_H \pm \Delta\omega_L$, above and below the resonance frequency in both polarizations. We take the width of the line to be defined by the frequencies above and below the resonance where the opacity for resonant scattering (eq. [17] of Langer and Rappaport 1982) is approximately equal to the Thomson opacity. This prescription gives the estimate,

$$\Delta\omega_L^2 \approx -\frac{\omega_H^2}{2}\left(\frac{\hbar\omega_H}{4mc^2}\right)\ln\left[7\times 10^{-4}B_{12}\left(\frac{\hbar\omega_H}{4mc^2}\right)^{1/2}\right],$$

where we have substituted $\hbar\omega_H/4$ for kT. More accurately, $\Delta\omega_L$ should vary with $kT(z)$ throughout the atmosphere, but we take $\Delta\omega_L$ constant to simplify the transfer scheme. The contribution to the emissivity from cyclotron line photons in the radiative transfer calculation is, therefore,

$$j_{\nu L}^i = \frac{1}{2\Delta\omega_L}\frac{\Lambda_L}{4\pi}, \tag{6}$$

where $i = 1, 2$ are the two polarization modes. We assume that both modes are resonant, and that half of the cyclotron line photons are produced in each mode.

Expressions for the Thomson and bremsstrahlung processes in a strong magnetic field have been calculated by Mészáros and Ventura (1979), Ventura (1979), and Nagel (1980). These are needed in the first place for finding the temperature and density structure of the atmosphere (radiative cooling), and in the second place for finding the spectrum. As in the nonmagnetic case, heating and cooling by the Compton energy exchange can be calculated with the coherent (magnetic) scattering cross section (see below). The *shape* of the spectrum should, however, be affected to some degree by incoherent scattering, especially at the resonance. The magnetized incoherent scattering is numerically very complicated, depending on angle of propagation rather sensitively (Nagel 1981*b*). Under those circumstances where the Compton effect represents a small fraction of the total cooling, we expect the spectral distortions to be relatively small over most of the spectrum. In this paper we proceed under this assumption and compute the continuum spectrum using the coherent scattering cross section, although in the energy balance, we do include the Compton energy losses and gains.

For finding the structure of the atmosphere we shall be using the expressions for the continuum opacities without the complication of the resonance, which is incorporated in the cyclotron line emissivity. Since we have a plane-parallel atmosphere, it is reasonable for the purposes of finding the atmospheric structure and the spectrum to use the two-stream approximation of the transfer equations, as in Mészáros, Nagel, and Ventura (1980). We use the following approximations to the angle-averaged, nonresonant opacities in a two-polarization magnetized plasma:

$$s_1 = n_e\sigma_T\left[\left(\frac{3}{4}\frac{1}{u}-\frac{1}{2u^2}\right)+\left(\frac{\ln u+\frac{1}{4}}{u}\right)\right][1-\Delta(\omega)] + \frac{1}{2}n_e\sigma_T\Delta(\omega),$$

$$s_2 = n_e\sigma_T\left[\left(\frac{2}{3}-\frac{5}{12u^2}\right)+\left(\frac{\ln u+\frac{1}{4}}{u}\right)\right][1-\Delta(\omega)] + \frac{1}{2}n_e\sigma_T\Delta(\omega),$$

$$s_{12} = s_{21} = n_e\sigma_T\left(\frac{\ln u+\frac{1}{4}}{u}\right)[1-\Delta(\omega)] + \frac{1}{4}n_e\sigma_T\Delta(\omega),$$

$$a_i = \frac{s_i}{n_e\sigma_T}\left[n_e^2 4\pi^2\alpha^3\frac{(hc/m_e)^2}{v_{th}}\left(\frac{1-e^{-\hbar\omega/kT}}{\omega^3}\right)\right], \tag{7}$$

for $\omega < \omega_H$, where $u = (\omega_H/\omega)^2$, and

$$\Delta(\omega) = \exp\left\{-\left[\frac{\omega-(\omega_H-\Delta\omega_L)}{\omega}\right]^2\right\}.$$

While for $\omega > \omega_H$, we take

$$s_i = \tfrac{1}{2}n_e\sigma_T,$$

$$s_{ij} = \tfrac{1}{4}n_e\sigma_T,$$

$$a_i = \frac{s_i}{n_e\sigma_T}\left[n_e^2 4\pi^2\alpha^3\frac{(hc/m_e)^2}{v_{th}}\left(\frac{1-e^{-\hbar\omega/kT}}{\omega^3}\right)\right]. \tag{8}$$

The Compton scattering opacity, s_i, and the bremsstrahlung opacity, a_i, are all measured in cm^{-1}, ω_H is the cyclotron circular frequency, σ_T is the Thomson cross section and $v_{th} \equiv (\pi kT/2m)^{1/2}$. We have taken into account the finite width of the resonance with the function $\Delta(\omega)$, which causes the cross sections to approach σ_T at $\omega_H - \Delta\omega_L$, the frequency at which the cyclotron photons are emitted in the lower line wing. Cyclotron photons are also emitted in the adjacent frequency bin $\omega_H + \Delta\omega_L$. These opacities are used in performing the two-stream radiative transfer calculation, layer by layer.

The bremsstrahlung emissivity is just $j_\nu^i = B_\nu^i a_\nu^i$, where B_ν^i is the Planck function for polarization i (one-half of the usual), and a_ν^i is the bremsstrahlung absorption coefficient when the Gaunt factors are set to unity. This expression plus the cyclotron line emissivity above is used as the emission coefficient in the radiative transfer equations. For the energy balance, we use the frequency-integrated bremsstrahlung emissivity,

$$\Lambda_B = \sum_{i=1}^{2} Q^i\rho^2 T^{1/2}(1-\langle\epsilon_\nu^i/\epsilon_{\nu B}^i\rangle)\ \text{ergs cm}^{-3}\ \text{s}^{-1}, \tag{9}$$

where we have accounted for inverse effects by including the term $\langle\epsilon_\nu^i/\epsilon_{\nu B}^i\rangle$, the ratio of the actual calculated radiation energy density per unit frequency in polarization i to the blackbody energy density $\epsilon_{\nu B}^i$, averaged over all frequencies. This approximate form is used in order to have the simpler dependence $\rho^2 T^{1/2}$ involving the two atmospheric parameters, this being the frequency-integrated expression of the emissivity. The reason for using this simpler expression is that in the

relaxation scheme, one has to take numerical derivatives of equation (9) and repeat, to find the equilibrium configuration. The values used for Q^i are

$$Q^1 = 0.6Q2x_H^{-2}[1 - e^{-x_H}(1 + x_H)], \quad Q^3 = 0.4Q, \quad (10)$$

where Q is the nonmagnetic value 5×10^{20} (Zel'dovich and Shakura 1969), and $x_H = h\nu_H/kT$. These Q^i are the frequency-integrated form of the approximate (magnetized) bremsstrahlung emissivities $j_\nu^1 \approx j_\nu^{NM} 0.6(\nu/\nu_H)^2 \exp(-h\nu/kT)$ and $j_\nu^2 \approx j_\nu^{NM} 0.4 \exp(-h\nu/kT)$, j_ν^{NM} being the nonmagnetic emissivity per unit frequency.

The inverse Compton cooling, in the nonmagnetic case, involves in the nonrelativistic approximation an expression of the type $\Lambda = c\sigma_T n_e U_{ph}(4kT/m_e c^2)$ ergs cm^{-3}, for electrons at temperature T, U_{ph} being a frequency-integrated photon energy density and σ_T the coherent Thomson cross section. The inverse effect can be taken into account by including the recoil (e.g., Kompaneets 1957), so that the average fractional photon energy change per scattering in the nonmagnetic case is $\Delta\nu/\nu = (4kT - h\nu)/m_e c^2$. In the strong magnetic field case, for $h\nu_H \ll m_e c^2$, one can expect that a similar expression involving the coherent magnetized scattering cross section will give the correct first-order Compton heating and cooling. We therefore write the net Compton cooling rate in ergs cm^{-3} s^{-1} as

$$\Lambda_C = \sum_{i=1}^{2} 8\sigma_T^{-1}\rho \int d\nu \sigma_\nu^i \epsilon_\nu^i (T - h\nu/4k), \quad (11)$$

where $\sigma_\nu^i = s^i/n_e$ from equations (7) and (8). In the approximation where ϵ_ν is isotropic, one can show from equilibrium considerations that the relative value of the terms accounting for direct and inverse effects should also be $(T - h\nu/4k)$, as in the nonmagnetic case discussed by Rybicki and Lightman (1979).

III. METHOD OF CALCULATION

We calculate the temperature and density structure of the atmosphere by setting up the equations of momentum and energy conservation in the presence of the ram pressure and heating by the infalling beam of protons, which is assumed to be initially monoenergetic, together with the two-stream magnetized radiative transfer equations. An initial guess for the atmospheric run of temperature and density is made, and the atmosphere is divided into homogeneous slabs (20–30) that conform stepwise to these initial guesses. The radiative transfer equation is solved layer by layer following the method described in the Appendix, and the radiation energy densities ϵ_ν^i for each slab are found. We then test each slab for energy balance by comparing the heating rate from the accreting protons with the total cooling rate given in § II*b*:

$$\phi \frac{dE}{dz}(\rho, T, E) = \Lambda(\rho, T, \epsilon^i), \quad (12)$$

where $\phi = \dot{M}/A$ is the proton flux, and $dE/dz = -\rho dE/dy$ as a function of (ρ, T, E) comes from our deceleration calculation (stored in tables). The quantity E is an average over the proton energy distribution, and $\Lambda(\rho, T, \epsilon^i)$ contains as a parameter the radiative energy densities ϵ_ν^i found by the transfer calculation. We also test for momentum balance,

$$\frac{dP}{dz} + \phi \frac{d\Pi}{dz}(\rho, T, E) + \frac{GM\rho}{(R_N + z)^2} = 0, \quad (13)$$

where $P = 2n_e kT$ is the thermal gas pressure, G is the gravitational constant, and the proton momentum deposition rate $d\Pi/dz = -\rho d\Pi/dy$ also comes from the tables. We have assumed radiation pressure to be unimportant (this can be verified after the solution is found). The proton energy E at the top of the atmosphere has the nonrelativistic value

$$E_0 = 134(M/M_\odot)(10^6 \text{ cm}/R_N) \text{ MeV}, \quad (14)$$

and the run of $E(z)$ is found by numerically integrating $dE(\rho, T, E)/dz$ slab by slab until E drops to zero. If E drops to zero inside a particular slab (i.e., not at a boundary), then dE/dz, $d\Pi/dz$ are redefined so that the energy and momentum with which the proton entered that slab is uniformly distributed over the width of that slab, and the stopping length is defined to lie at the midpoint of the slab. The last proton-heated slab is considered to be the bottom of the atmosphere. Each layer, or slab, including the bottom one, is assumed to radiate both upward and downward. The bottom layer has as boundary condition that of total reflection, while the top one has that of no incoming radiation from above. These boundary conditions allow us to solve the transfer equations layer by layer (see Appendix). They imply also that no radiant energy is transported inward into the star (radiated downward from the bottom slab), though in reality there may be some loss of energy into the stellar surface.

The equilibrium solution is found iteratively. If momentum and energy are not balanced for the density and temperature run of iteration j, we choose a new $(j + 1)$th guess of the run of variables by using a relaxation technique, a simple description of which is found, for instance, in Clayton (1968). One differentiates the force and energy equations in the variables (ρ and T) to be varied, inserting the energy and momentum deficit found from equations (12) and (13) in iteration j, to find $\Delta\rho_{j+1}$, ΔT_{j+1}, which are then added to ρ_j, T_j. The proton-stopping calculation is repeated to find the new heating rate and ram force in each slab. The radiation transfer is also repeated each iteration in order to obtain the new ϵ_ν^i for the atmosphere. Although the numerically obtained photon energy densities ϵ_ν^i also depend on T and ρ, derivatives of ϵ_ν^i cannot be calculated analytically. Differences are used to approximate the derivatives of ϵ_ν^i, but there is still some degree of uncertainty, which slows down the convergence. We were, however, able to achieve balance in equations (12) and (13), in all cases, to an accuracy of at least 10% in each slab and in most cases to much better than 10%. The slabs are fixed in space during the iteration so that the Δz_j are constant, and the y_j are recalculated with each change in ρ_j. The top slab is assumed to have a density given by the free-fall value,

$$n_0 = 2 \times 10^{19} \left(\frac{\dot{M}}{10^{16} \text{ g s}^{-1}}\right)\left(\frac{10^{10} \text{ cm}^2}{A}\right) \text{cm}^{-3}, \quad (15)$$

and this value acts as a boundary condition. The free-fall density is chosen as a reasonable upper boundary of the atmosphere since above this point the density of the static atmosphere would fall below that of the infalling proton beam.

This choice does not assign a density to a fixed distance above the stellar surface, because the spatial extent of the atmosphere, z_0, is determined by the point at which the proton beam stops. Since the protons do not necessarily stop in the last slab of our numerical grid, the bottom of the atmosphere varies during the iteration. The variations in slab $(j + 1)$ are found as a function of those of slab j and the energy and momentum deficits, so that the atmosphere balances from top to bottom. The final spectrum is then calculated for the equilibrium atmosphere, using the exact cross sections.

The calculation of the beaming of the radiation requires an angle-dependent transfer scheme. We use the integral equation method for a magnetized medium (Mészáros and Bonazzola 1981). Knowing the temperature and density of each slab, we use the upward directed, angle-dependent intensity from each slab as the input for the slab above, which then rescatters this beam of radiation, as well as itself contributing some emission and absorption. The scattering is assumed to be coherent, and the bottom slab was assumed to be only self-radiating. This method is expedient, in view of the numerical magnitude of the task, but it involves the approximation of neglecting the backward-scattered radiation. For most of the frequency and magnetic field values involved in these calculations, the dominant polarization is extraordinary, for which $\tau \leq 1$. In this case, the approximation of neglecting backscattered radiation does not introduce a large error. In addition, a property of the magnetized scattering cross sections is that they approximate fairly well the case of complete angular redistribution (Nagel 1981*a*). For those frequencies where $\tau > 1$, complete redistribution ensures that scattered photons lose information about their previous directionality, so that the inaccuracy incurred is mostly in the total intensity calculated at the top, but not in the calculated angular structure. For this reason, the beam structure and pulse profiles are normalized to unit intensity, while the total intensity and spectra are calculated by the two-stream approximation, which has a full treatment of the boundary conditions.

IV. RESULTS

The free parameters determining the structure of the atmosphere are the accretion rate $\dot{M}$, the neutron star mass M and radius R_N, the surface magnetic field strength B, and the escape probability of line photons $P_{\rm esc}$. The procedure described in § III has been carried out for four accretion rates, $\dot{M} = 10^{14}$, 10^{15}, 10^{16}, 10^{17} g s^{-1}, and four values of the magnetic field strength, $B = 2.5 \times 10^{12}$, 5×10^{12}, 10^{13}, 2×10^{13} G, with the other parameters for the most part held constant at the values $M = 1\,M_\odot$, $R_N = 1.2 \times 10^6$ cm, $P_{\rm esc} = 1$. These values of M and R_N are chosen to give $E_0 = 115$ MeV by equation (14) to match the initial energy, corresponding to $v = c/2$, of the proton stopping calculations.

Figure 2 shows the equilibrium temperature and density profiles for an accretion rate of $\dot{M} = 10^{15}$ g s^{-1} and four different values of magnetic field strength. The cyclotron resonance frequency, depending on the magnetic field as $\hbar\omega_H = 12B_{12}$ keV, acts as a thermostat which determines the equilibrium value of the electron temperature. As a result of the exponential dependence of the cyclotron photon production rate on T (cf. eq. [5]), cyclotron cooling becomes very effective when temperatures in the atmosphere approach $kT = \hbar\omega_H$. The equilibrium temperatures are therefore extremely sensitive

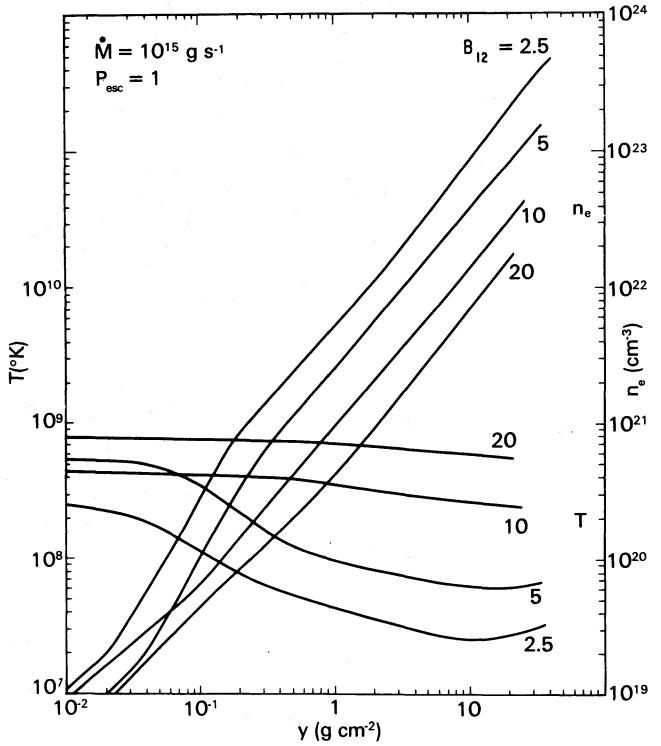

FIG. 2.—Atmospheric temperature and density profiles for different magnetic field strengths in units of 10^{12} G, plotted against $y = -\int_\infty^z n_e(z)m_p\,dz$. Infall is from the left.

to B and are always less than $\hbar\omega_H$. At the bottom of the atmosphere (large y), bremsstrahlung and cyclotron line emission are the dominant cooling mechanisms, with the relative contributions a function of B. For $B = 2.5 \times 10^{12}$ G, cyclotron emission makes up less than 10% of the total cooling, whereas for $B = 2 \times 10^{13}$ G, it contributes nearly 90%, with a sharp increase in the cyclotron cooling contribution between 5×10^{12} G and 10^{13} G. Although this result would seem at first to contradict the behavior of the cyclotron line cooling expression (cf. eq. [5]) as a function of B, the relative contribution of line cooling actually depends on the ratio of the equilibrium kT to $\hbar\omega_H$. As it turns out, equilibrium atmospheric temperatures rise with increasing B faster than the corresponding rise in $\hbar\omega_H$. The ratio, $kT/\hbar\omega_H$, therefore increases with increasing B, giving a larger line-cooling contribution. At the top of the atmosphere (small y), Compton cooling dominates, because of the dependence on n_e rather than n_e^2, as is the case for bremsstrahlung and cyclotron cooling. Compton heating makes a significant contribution to the energy balance for the higher field strengths, where a large number of cyclotron line photons are produced with energies higher than that of the atmospheric electrons. When these photons scatter on their way out of the atmosphere, they give a portion of their energy back to the electrons.

The density profiles have a roughly linear dependence on y (exponential in z), which is characteristic of an isothermal atmosphere in hydrostatic equilibrium, with departures due to the temperature gradients in the atmosphere. Scale heights vary from 50 cm for $B = 2.5 \times 10^{12}$ G to 200 cm for $B = 2 \times 10^{13}$ G. The depth of the atmosphere is the stopping

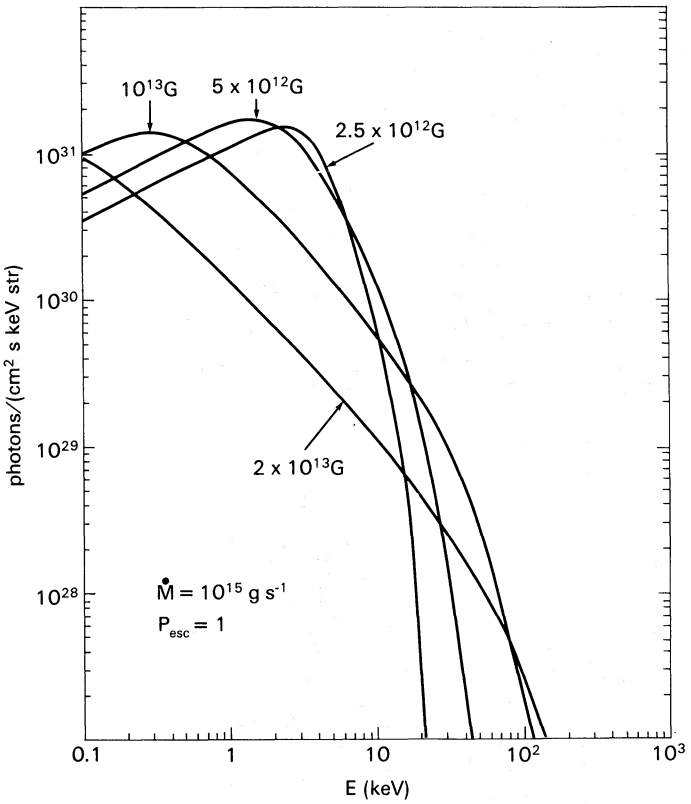

FIG. 3.—Photon number spectra for the atmospheres of Fig. 2, labeled with different values of the magnetic field strength. Only the continuum spectra are shown, although additional photons are also produced at the cyclotron frequency, which has the values 30, 60, 120, and 240 keV for these cases.

distance of the protons, y_0. The stopping distances decrease with increasing magnetic field mainly because the proton energy deposition rates increase with T (cf. Fig. 1). Since the optical depth of the atmospheres are directly proportional to the stopping distance,

$$\tau \approx \sigma y_0/m_p = 6(\sigma/0.5\sigma_T)(y_0/30 \text{ g cm}^{-2}) , \qquad (16)$$

atmospheres with higher magnetic fields should be more optically thin.

This is indeed the case, as is shown in Figure 3, where we have plotted the spectrum of radiation emerging from the top of the atmospheres of Figure 2. The lower field strength photon spectra have a Rayleigh-Jeans behavior up to around 3 keV, which is the equivalent blackbody temperature, and fall off steeply at higher energies, indicating higher optical depths. The atmospheres with $B > 5 \times 10^{12}$ G have spectra which begin to resemble optically thin thermal bremsstrahlung: power laws of index -1 with high energy cutoffs. Figure 3 shows only the continuum part of the emergent spectrum. Because of our approximate treatment of the cyclotron line radiation transfer, we have no accurate information on the appearance of an observable emission (or absorption) line in the spectrum. Although the calculation gives the number of photons appearing in the line wings, it does not follow the energy redistribution of these line photons as they scatter into the adjacent continuum. A fraction of the line photons may diffuse down to (at most) frequencies $\hbar\omega \gtrsim k\langle T_e\rangle$. We therefore show only the spectrum of the continuum photons, keeping in mind that above $\sim 0.5\hbar\omega_H$ this gives only a lower limit on the photon number.

The contribution of the two polarization modes to the continuum spectrum is shown in Figure 4, which includes the vacuum polarization effect as do all other cases. This effect is due to the presence of virtual e^+e^- pairs induced by the strong magnetic field (Mészáros and Ventura 1978, 1979), which cause the polarization eigenmodes to change from circular to linear at the energy $\hbar\omega_v \approx 3$ keV $(n_e/10^{22}\text{ cm}^{-3})^{1/2}(4 \times 10^{12}\text{ G}/B)$. Above this energy, the vacuum dominates over the plasma in determining how radiation propagates in the medium and causes both modes to be resonant at the cyclotron frequency if $\omega_v < \omega_H$. At low frequencies ($\omega < \omega_v$) and at $\omega \gtrsim \omega_H$, where the plasma dominates, we can label the modes in the conventional manner, with mode 1 being the extraordinary and mode 2 being the ordinary mode. In the vacuum-dominated region, $\omega_v < \omega < \omega_H$, modes 1 and 2 do not correspond to the extraordinary and ordinary modes as usually defined. The convention used here is the same as in Mészáros and Bonazzola (1981). The "vacuum feature" at $\hbar\omega_v$, found by Ventura, Nagel, and Mészáros (1979) in spectra computed for homogeneous atmospheres, does not appear in these spectra because of the density gradients, which spread $\hbar\omega_v$ over a range of frequencies. If, however, each polarization were measured separately, one would see different modes predominate above and below ω_v, as shown in Figure 4.

The atmospheric structure and spectrum are much less sensitive to the value of the accretion rate. Figure 5 shows the temperature and density profiles for four values of $\dot{M}$ with B held constant at 5×10^{12} G. In contrast to the large variation of temperature with varying B (cf. Fig. 2), the temperatures change only slightly with varying $\dot{M}$. The stopping distances

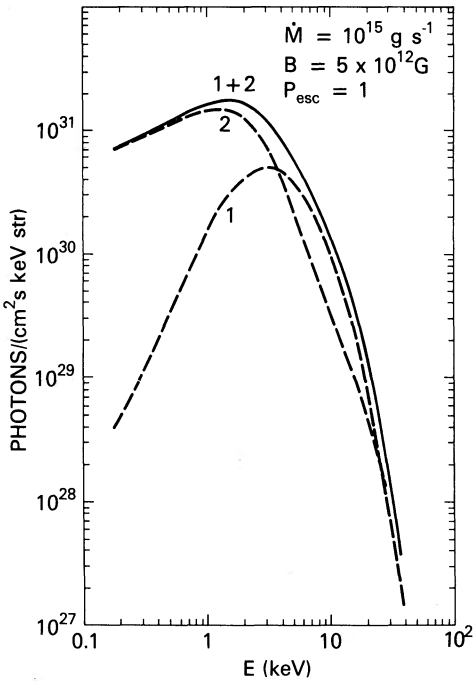

FIG. 4.—Photon number spectrum for the case $B = 5 \times 10^{12}$ G, showing the spectra of individual polarization modes (1 ≡ extraordinary, 2 ≡ ordinary).

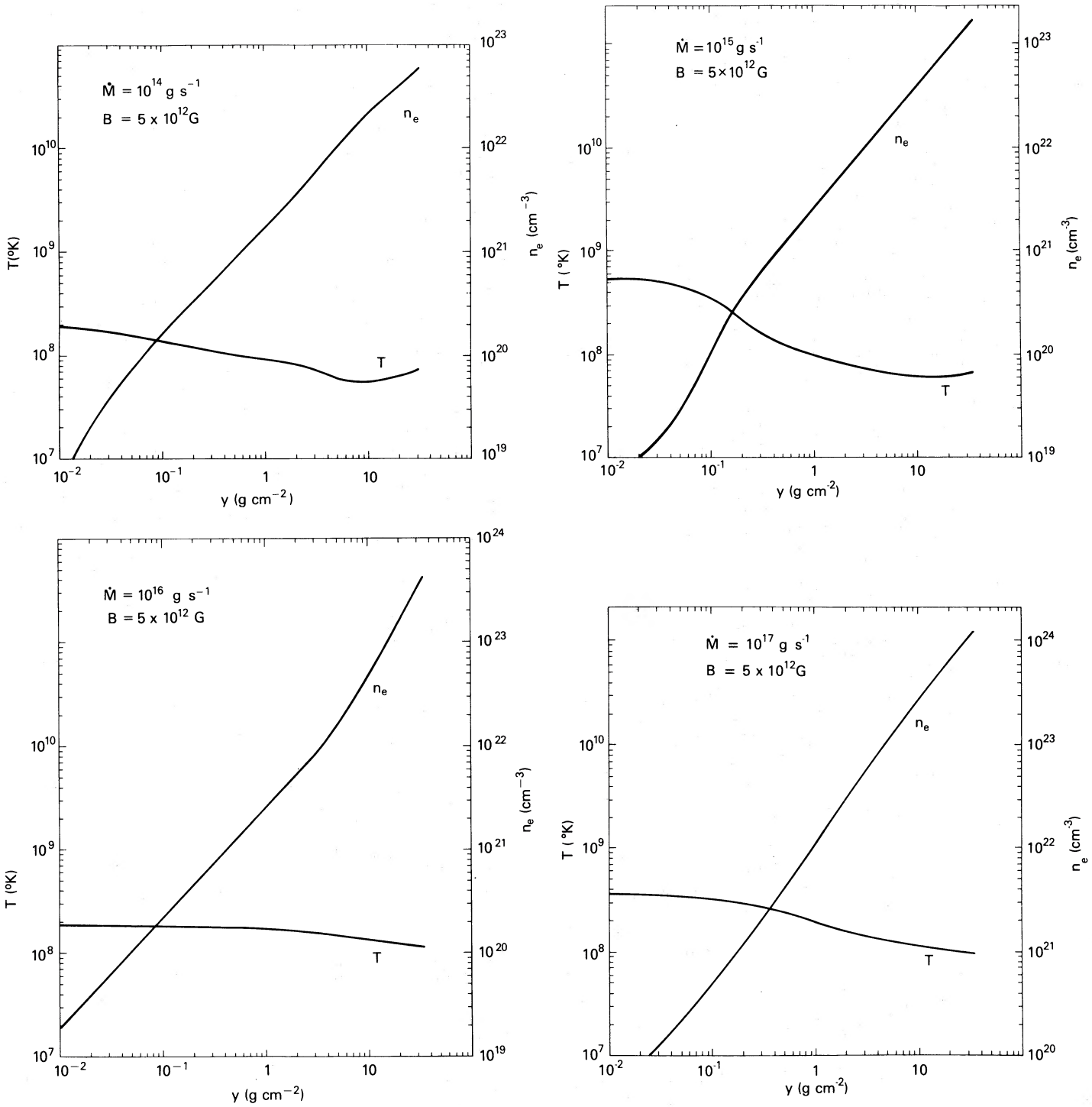

FIG. 5.—Atmospheric temperature and density profiles for different accretion rates and constant field strength $B = 5 \times 10^{12}$ G

are similar for all four cases, with a small increase ($y_0 = 20$–30 g cm^{-2}) with increasing $\dot{M}$. The main effect of increasing $\dot{M}$ is to increase the density at the bottom of the atmosphere. There is also, therefore, a decrease in the scale height, since y_0 is roughly constant, to a value of only ~ 10 cm for $\dot{M} = 10^{17}$ g s^{-1}. Although we have neglected the effects of radiation pressure in calculating the atmospheric structure, we are able to compute the value of the radiation pressure in the equilibrium atmospheres from the radiative transfer. We find that it is small relative to the gas pressure for $\dot{M} \lesssim 10^{16}$ g s^{-1} but estimate that it becomes comparable to the gas pressure at the top of the atmosphere for $\dot{M} = 10^{17}$ g s^{-1}. Therefore, we may not be justified in neglecting radiation pressure for $\dot{M} = 10^{17}$ g s^{-1}, although for the lower accretion rates, the assumption seems to be valid. An accurate calculation of the radiation pressure at high $\dot{M}$ would require a more detailed treatment of the line photon frequency redistribution.

Figure 6 shows that there is very little difference in the continuum spectra emerging from the atmospheres with varying $\dot{M}$, at least in the approximation of coherent scattering. This is not surprising, since it is the optical depth (proportional to the equilibrium value of y_0) which determines the shape of the spectrum, and y_0 does not vary much with accretion rate. The relative contribution of cyclotron line emission to the cooling *does* vary significantly with $\dot{M}$. For $\dot{M} = 10^{14}$ g s^{-1}, line cooling makes up 11% of the total cooling, whereas for $\dot{M} = 10^{16}$ g s^{-1}, it represents almost 95% of the total. Compton heating makes a significant negative contribution to the total for $\dot{M} \gtrsim 10^{16}$ g s^{-1}, so that the spectra for the highest accretion rates may look different with the inclusion of incoherent scattering. Since the photons which are responsible for most of the Compton heating are line photons, these photons would lose energy in the scattering process and enhance the continuum below the line. This missing contribution could represent up to 95% of the total luminosity, and could produce significant differences in the spectrum as a function of accretion rate, at the higher $\dot{M}$ values.

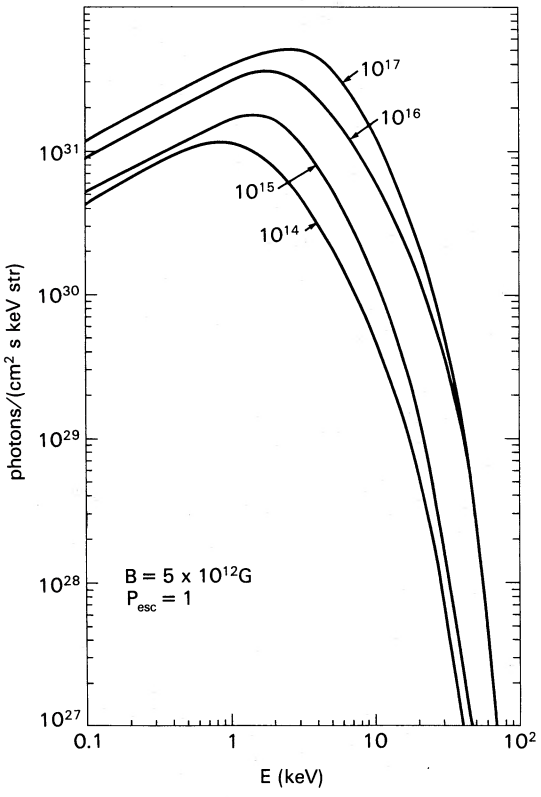

FIG. 6.—Photon number spectra for the atmospheres of Fig. 5, labeled with different values of the accretion rate in g s^{-1}. The cyclotron frequency for all cases is 60 keV.

We have so far presented results for cases where $P_{esc} = 1$, meaning that line photons have a 100% probability of escaping without absorption. Cases where $P_{esc} = 0.1$ were also investigated and were not found to produce significantly different results from the $P_{esc} = 1$ cases for the same values of B and $\dot{M}$. The reason this is so lies in the approximate exp $(-\hbar\omega_H/kT)$ dependence of the line photon production rate. It is possible for a small increase in T to counteract an order-of-magnitude difference in P_{esc}, such that the line cooling remains the same (i.e., 10 times more line photons are produced but only one-tenth of them escape). The increase in T necessary to do this is small enough to produce little observable difference in the T profile or the spectrum.

We have plotted in Figure 7 the pulse shape, normalized in each case to unit intensity, for different values of B, frequency, and aspect angles (ϕ_1, ϕ_2). The aspect angles are the angle between the magnetic and rotation axis, and that between the line of sight and the rotation axis. The pulse shapes are symmetric to an interchange of ϕ_1 and ϕ_2. The pulse shapes, produced by the radiation passing through atmospheres of decreasing density and slowly increasing temperature, can be compared with those coming from homogeneous atmospheres. The present pulses resemble qualitatively those coming from a uniform, self-radiating slab, with no background illumination, discussed by Mészáros and Bonazzola (1981). Of course, in those previous calculations, the choice of temperature and density was arbitrary. One can see, however, that different temperature gradients produce different pulse shapes, so that a uniform atmosphere at a density and temperature of the bottom slab would still be only a rough approximation.

The pencil beam pulses from these Coulomb-heated atmospheres are characterized over a significant range of aspect angles by single pulse shapes at high frequencies and notched or multiple pulse shapes at low frequencies. The energy at which the pulses undergo this metamorphosis is $\hbar\omega \sim \hbar\omega_H/4$. The pulses therefore become multiple at higher energies for higher field strengths, where ω_H is larger (cf. Fig. 7). The notches occur at phase zero, when the observer is looking down the magnetic pole. At this angle, the magnetized cross sections undergo a minimum at frequencies below ω_H. If the optical depth of the atmosphere is not too large, the outgoing intensity will be directly proportional to the emissivity, which has the same angle and frequency dependence as the cross sections. The intensity will thus have a minimum at phase 0. If the atmosphere is optically thick, the intensity is inversely proportional to the cross section, and the notches tend to disappear (Nagel 1981*a*). The notches in the higher magnetic field cases are therefore more pronounced as a result of the lower optical depth.

The spectral index is a function of phase, since the intrinsic beam shape is both angle and frequency dependent. As previously found in homogeneous slab models (Mészáros and

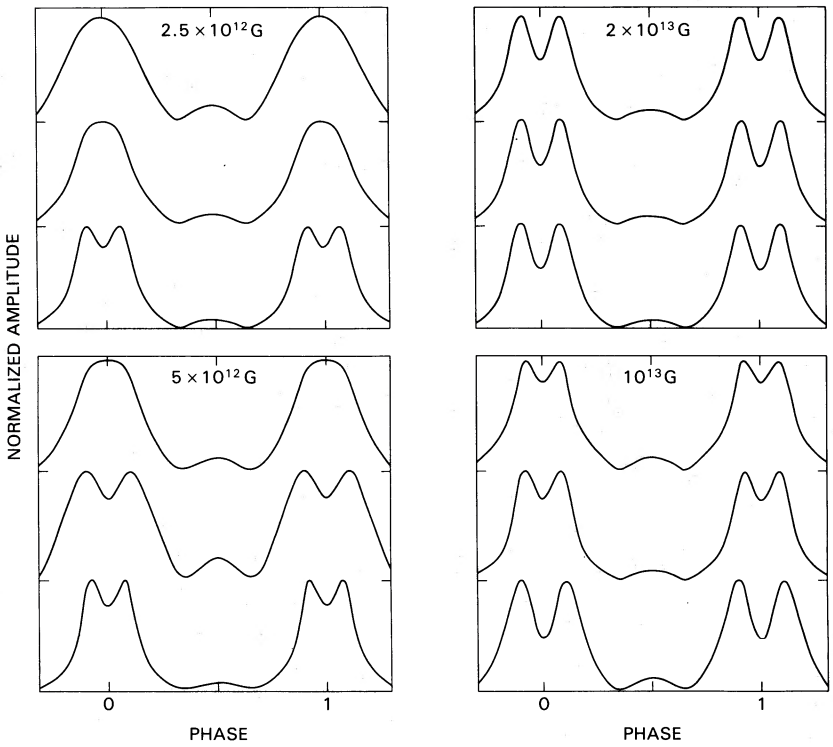

FIG. 7.—Normalized pulse shapes for aspect angles (60°, 45°), $\dot{M} = 10^{15}$ g s^{-1}, $P_{esc} = 1$, and four different values of magnetic field strength, each at three photon energies: 18, 10, and 3 keV, from top to bottom.

Bonazzola 1981; Nagel 1981*a*), the spectral indices for most aspect angles are hardest at midpulse. In Figure 8, we have plotted the spectral index as a function of pulse phase for the pulses in Figure 7. The spectra for $B = 5 \times 10^{12}$ G show a hardening toward phase 0 (midpulse) for the energy range 10–18 keV, where the pulses are developing notches, but none in the energy range 3–10 keV, where the pulse shapes are stable. Similarly, the spectra for $B = 10^{13}$ G show a hardening toward midpulse only in the lower energy range, where the pulse notches are deepening.

V. DISCUSSION

We have investigated the structure of accreting atmospheres where the *main* deceleration mechanism of the infalling protons is distant Coulomb encounters with atmospheric electrons. We *assume* that a collisionless shock does not arise, although *a priori* one can only make plausibility arguments (e.g., Kirk and Trümper 1982). The alternative approach of calculating an accreting magnetized atmosphere when a collisionless shock does occur has been explored by Langer and Rappaport (1982), while the effects of radiation pressure including approximate magnetic cross sections were explored by Wang and Frank (1981). Earlier work by Basko and Sunyaev (1976) assumed a magnetic field to determine the geometry of the accretion column but used nonmagnetic cross sections. These atmospheres with a collisionless shock or with strong radiation pressure (which produces a quasi shock) differ radically from what we have calculated here, since the shock stands off from the stellar surface at a distance Δz which is comparable to or larger than the transverse dimension of the accretion column. The optical depth across B can be less than that along B,

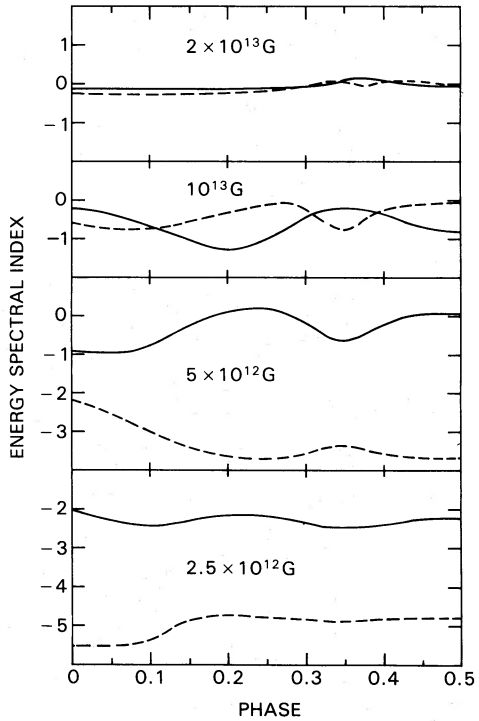

FIG. 8.—Energy spectral index α, defined by $dL = KE^{\alpha}dE$, as a function of pulse phase, in two different energy ranges: 3–10 keV (*solid lines*) and 10–18 keV (*dashed lines*), for aspect angles (60°, 45°).

so that radiation escapes from the sides of the column, forming fan beam pulses. The Coulomb-heated atmospheres, on the other hand, have Δz much less than the polar cap radius, which allows us to use the convenient plane-parallel approximation.

We find that Coulomb-heated atmospheres are indeed thin slabs with scale heights of only ~ 10–200 cm, much smaller than the polar cap radii $R_p \sim 10^4$–10^5 cm determined from the accretion flow. Very little radiation would be expected to escape from the sides of the slab, since the optical depths are ~ 1000 times greater in this direction than along the magnetic pole. Densities are quite high (10^{22}–10^{24} cm^{-3}) at the base of the atmosphere, with the highest densities occurring for low field strengths and high accretion rates.

The equilibrium stopping distances are in the range $y_0 \approx 20$–50 g cm^{-2}, with the longer stopping distances occurring for low field strengths and low accretion rates. In the cases where $y_0 \approx 50$ g cm^{-2}, nuclear collisions, which were included in the energy deposition rate, play a significant role in slowing down the protons in the accretion flow. If the Coulomb energy deposition rates used in the present calculation are overestimates, then nuclear collisions could be expected to be important for the higher field strength cases also, the values of y_0 would be higher, ~ 50 g cm^{-2}, and the continuum spectra would be more optically thick. The spectra for the low field strengths would not change much since these cases have y_0 close to 50 g cm^{-2} even with the present Coulomb rates.

Cyclotron line cooling is very important in determining the equilibrium temperature of the atmosphere. Because of the $\sim \exp(-\hbar\omega_H/kT)$ dependence in the production rate of line photons by collisional excitations, the equilibrium temperatures are extremely sensitive to the magnetic field strength. As the field increases, line cooling contributes more and more to the total cooling, but it becomes less effective in keeping the temperature low. As $\hbar\omega_H$ moves up into the greater than 200 keV range, as is the case for $B = 2 \times 10^{13}$ G, equilibrium temperatures approach 10^9 K, where pair production (either photon-photon or photon–magnetic field) could become an important cooling mechanism. It is therefore unlikely that in these equilibrium atmospheres, temperatures could greatly exceed $\sim 10^9$ K.

We have neglected the excitation of electrons to Landau levels higher than the first excited state. This could become important at low field strengths, if the energy and spacing of the electron states are small compared with the equilibrium temperature in the atmosphere. It is even possible in very low fields for the first few cyclotron harmonics to become optically thick, so that the cooling contribution would come from a higher transition (the lowest optically thin transition). However, for the range of field strengths we have considered, the temperatures are all well below the energy of the first excited state. Furthermore, radiative de-excitation is so rapid compared with collisional processes that very few electrons would be expected to be excited from the first to the second excited state. In addition, bremsstrahlung is so effective for low field strengths that even for fields below 2.5×10^{12} G, there may be no need to consider cyclotron cooling from any but the lowest excited state.

We have also neglected the changes in energy of the photons as they Compton scatter, though we do take into account the Comptonization of the electrons in the cooling part of the energy balance. Although the change in energy of a photon is small in each scattering event, each photon may undergo many scatterings in the atmosphere before it escapes. One indicator of the importance of these incoherence effects is the contribution of Compton scattering to the total cooling, since the energy gained or lost by the electrons must equal that of the photons. For the equilibrium atmospheres we have presented, Compton scattering makes up about 30% of the cooling or heating, except for $\dot{M} \geq 10^{16}$ g s^{-1}, where the percentage is somewhat higher. However, most of this contribution is heating by line photons and not scattering of continuum photons. The cooling by lower energy continuum photons at the top of the atmosphere represents only a few percent of the total cooling, so the continuum spectrum below $\sim 0.5\hbar\omega_H$ is unlikely to be seriously affected. The main consequences of neglecting incoherence effects, therefore, are poor information on the shape of the line and an underestimate of the continuum level immediately below the line. We may also have somewhat overestimated Compton heating by line photons in preventing these photons from losing energy as they scatter. As they blend into the continuum, they should become less effective in heating electrons.

A number of observed X-ray pulsars have hard power-law spectra with turnovers at around 10–20 keV (Rose *et al.* 1979; Pravdo *et al.* 1979; Becker *et al.* 1977; Pravdo *et al.* 1978). In several sources, such as OA 01653−40 and 4U 1145−61, the power-law spectra show evidence only for a slight steepening above 20 keV, indicating the presence of higher temperatures. Many of these pulsars show broad line features in their spectra at energies between 6.6 and 7 keV which have been identified as Fe emission. Only two pulsars, however, show clear evidence for cyclotron line features in their spectra: Her X-1 and 4U 0115+63 (Voges *et al.* 1982; White, Swank, and Holt 1983). Our calculations suggest that some of the pulsars having hard power-law spectra without cyclotron features may have higher magnetic fields. A spectrum with index -1 extending to 30–50 keV before steepening requires $B > 5 \times 10^{12}$ G; the cyclotron frequency would be at $\hbar\omega_H > 60$ keV, above the sensitivity of most detectors. The spectra for $B \leq 5 \times 10^{12}$ G fall off steeply in the 10–30 keV range, although the downscattering of resonance photons could change the shape of the spectrum in this region.

The best observational evidence for slab atmospheres which produce pencil beam pulses comes from the observed frequency dependence of pulse shapes. Many X-ray pulsars show transitions from single pulses at high frequency to multiple pulses at low frequencies, without phase shifts (Pravdo *et al.* 1977; White, Swank, and Holt 1983), as well as a spectral hardening toward midpulse. Since our calculations predict this transition to occur at $\sim \frac{1}{4}$–$\frac{1}{3}\hbar\omega_H$, an independent observational estimate of B is possible. This is a higher transition frequency than predicted by Mészáros and Bonazzola (1981) for semi-infinite homogeneous atmospheres. The exact fraction of the cyclotron frequency below which the pulse splits depends on the viewing angle.

Since we now have spectral, pulse shape, and phase-spectroscopic predictions from one of the two main X-ray pulsar models (for $L_X \lesssim 10^{37}$ ergs s^{-1}), the time seems ripe for a more detailed comparison with the data. From the preliminary comparison we have made, there seem to be several overall similarities between some X-ray pulsars and our

models, which is encouraging. One should bear in mind, however, that there are departures from the "average" observed behavior, in addition to the fact that the range of applicability of our model, $L_X < 10^{37}$ ergs s^{-1}, reduces the total available sample.

consistent column atmosphere has been given by Langer and Rappaport (1982), which may also fit some observed X-ray pulsar spectra. While pulse shapes and spectral index versus phase predictions have not yet been made for the shock models, previous work on non-self-consistent column atmospheres suggests that the resulting fan-beam pulses may be rather broad (Yahel 1980; Pravdo and Bussard 1981; Nagel 1981*a*). This may be inconsistent with many pulsars, but determinations of the pulse shapes for self-consistent shock atmospheres are needed before one can decide on this issue.

As the volume of theoretical predictions from the shock and Coulomb models grows along with observational data on X-ray pulsars, statistical tests of consistency may be very fruitful. In this respect, the organization of available observational material on spectra, pulse shape, and pulse phase spectroscopy for as many X-ray pulsars as possible, as provided by White, Swank, and Holt (1983), is of great value. We may then be able to decide, from consistency tests, in favor of one model or the other. Detailed comparison with model predictions could furthermore yield extremely useful information on physical parameters in the accreting atmospheres, such as magnetic field strength, temperature, and density.

The authors would like to thank D. Q. Lamb, F. K. Lamb, S. Langer, W. Nagel, J. Swank, N. White, and J. Ventura for useful comments. P. M. is grateful to NASA GSFC and the University of Maryland for support in the initial phases of this work and acknowledges additional support from NASA grant NAGW-246.

APPENDIX

RADIATIVE TRANSFER IN AN INHOMOGENEOUS ATMOSPHERE

Mészáros, Nagel, and Ventura (1980) have given solutions of the transfer equations for polarized radiation in a strongly magnetized, self-radiating homogeneous slab. We use these results to numerically solve the one-dimensional transfer problem in the two-stream approximation for an inhomogeneous plane-parallel atmosphere. As discussed in § V, the Coulomb-heated atmospheres have scale heights which are much smaller than their cross-sectional diameters, and so both the plane-parallel and the two-stream approximations should be quite good.

We denote the upgoing and downgoing intensities in the orthogonal polarization modes 1 and 2 by J_1, J_2, K_1, K_2, respectively. The slab has a width z_0, with $z = 0$ at the stellar surface, and is divided into N layers, each having a constant temperature, density, and fixed width Δz_n. The solutions to the transfer equations which are given by Mészáros, Nagel, and Ventura (1980) give the intensities in each layer. The solutions in layer n at each frequency can be written in the matric form:

$$\mathbf{I}_n(z) = \boldsymbol{\xi}_n + A_n(z)\mathbf{C}_n \,, \tag{A1}$$

where

$$\mathbf{I}_n(z_n) = \begin{bmatrix} J_1^n(z_n) \\ J_2^n(z_n) \\ K_1^n(z_n) \\ K_2^n(z_n) \end{bmatrix}, \qquad \boldsymbol{\xi}_n = \begin{bmatrix} \xi_1^n \\ \xi_2^n \\ \xi_1^n \\ \xi_2^n \end{bmatrix}, \qquad \mathbf{C}_n = \begin{bmatrix} C_1^n \\ C_2^n \\ C_3^n \\ C_4^n \end{bmatrix}.$$

The $\mathbf{C}_n$ are undetermined coefficients, the 4×4 matrices $A_n(z)$ involve combinations of scattering and absorption coefficients multiplied by exponentials in z, and $\boldsymbol{\xi}_n$ is the free-free and the cyclotron line emission in the layer. The solutions in each layer involve four unknown coefficients; and N layers minus four boundary conditions gives a total of $4N - 4$ unknowns. We solve for these $4(N - 1)$ coefficients simultaneously by matching the intensities at each of the $(N - 1)$ boundaries. The boundary conditions on the intensities at $z = z_n$ can then be written

$$\boldsymbol{\xi}_{n-1} + A_{n-1}(z_n)\mathbf{C}_{n-1} = \boldsymbol{\xi}_n + A_n(z_n)\mathbf{C}_n \,. \tag{A2}$$

As discussed in Harding and Tademaru (1981), simultaneous equations of this form can be solved without inverting $N \times N$ matrices by writing the coefficients in layer N in terms of those in layer 1 as

$$A_N(z_N)\mathbf{C}_N = M_N A_1(z_2)\mathbf{C}_1 + \boldsymbol{\chi}_N \,, \tag{A3}$$

where

$$\boldsymbol{\chi}_N = \sum_{n=2}^{N} \prod_{m=n}^{N-1} A_m(z_{m+1})A_m^{-1}(z_m)(\boldsymbol{\xi}_{n-1} - \boldsymbol{\xi}_n) \qquad \text{and} \qquad M_N = \prod_{n=2}^{N-1} A_n(z_{n+1})A_n^{-1}(z_n) \,.$$

We choose the boundary conditions to be

$$K_{1,2}^N = 0 \,, \quad J_{1,2}^1 = K_{1,2}^1 \,. \tag{A4}$$

That is, no radiation is incident on the slab from above, and the downgoing radiation in the bottom slab is totally reflected. With these boundary conditions, the problem of finding the intensities emerging from the top and bottom of the slab has been reduced to solving the set of four simultaneous equations (A3). The intensities in all other layers can then easily be determined from the bottom layer up using equation (A2).

REFERENCES

Alme, M. L., and Wilson, J. R. 1973, *Ap. J.*, **186**, 1015.
Basko, M. M., and Sunyaev, R. A. 1975, *Astr. Ap.*, **42**, 311.
———. 1976, *M.N.R.A.S.*, **175**, 395.
Becker, R. H., Rothschild, R. E., Boldt, E. A., Holt, S. S., Pravdo, S. H., Serlemitsos, P. J., and Swank, J. H. 1977, *Ap. J.*, **222**, 912.
Bonazzola, S., Heyvaerts, J., and Puget, J. L. 1979, *Astr. Ap.*, **78**, 53.
Bussard, R. W. 1980, *Ap. J.*, **237**, 970.
Bussard, R. W., and Lamb, F. K. 1982, in *Gamma Ray Transients and Related Astrophysical Phenomena*, ed. R. E. Lingenfelter, H. S. Hudson, and D. M. Worrall (New York: AIP), p. 189.
Clayton, D. D. 1968, *Principles of Stellar Evolution and Nucleosynthesis* (New York: McGraw-Hill).
Emslie, A. G. 1980, *Ap. J.*, **235**, 1055.
Harding, A. K., and Tademaru, E. 1981, *Ap. J.*, **243**, 597.
Kirk, J. G. 1980, *Plasma Phys.*, **22**, 639.
Kirk, J. G., and Galloway, D. J. 1981, *M.N.R.A.S.*, **195**, 45.
———. 1982, *Plasma Phys.*, **24**, 339.
Kirk, J. G., and Mészáros, P. 1980, *Ap. J.*, **241**, 1153.
Kirk, J. G., and Trümper, J. 1982, in *Accretion Driven Stellar X-Ray Sources*, ed. W. H. G. Lewin and E. P. J. van den Heuvel (Cambridge: Cambridge University Press).
Kompaneets, A. S. 1957, *Soviet Phys.—JETP*, **4**, 730.
Lamb, F. K., Pethick, C. J., and Pines, D. 1973, *Ap. J.*, **184**, 271.
Langer, S. H., McCray, R., and Baan, W. A. 1980, *Ap. J.*, **238**, 731.
Langer, S. H., and Rappaport, S. 1982, *Ap. J.*, **257**, 733.
McCray, R., and Lamb, F. K. 1976, *Ap. J. (Letters)*, **204**, L115.
McKee, C. F. 1970, *Phys. Rev. Letters*, **24**, L990.
Mészáros, P., and Bonazzola, S. 1981, *Ap. J.*, **251**, 695.
Mészáros, P., Harding, A. K., Kirk, J. G., and Galloway, D. J. 1983, *Ap. J. (Letters)*, **266**, L33.
Mészáros, P., Nagel, W., and Ventura, J. 1980, *Ap. J.*, **238**, 1066.
Mészáros, P., and Ventura, J. 1978, *Phys. Rev. Letters*, **41**, 1544.
———. 1979, *Phys. Rev. D*, **19**, 3565.
Nagel, W. 1980, *Ap. J.*, **236**, 904.
———. 1981*a*, *Ap. J.*, **251**, 278.
———. 1981*b*, *Ap. J.*, **251**, 288.
Pavlov, G. G., and Yakovlev, D. G. 1976, *Soviet Phys.—JETP*, **43**, 389.
Pravdo, S. H., Boldt, E. A., Holt, S. S., and Serlemitsos, P. J. 1977, *Ap. J. (Letters)*, **216**, L23.
Pravdo, S. H., and Bussard, R. W. 1981, *Ap. J. (Letters)*, **246**, L115.
Pravdo, S. H., Bussard, R. W., Becker, R. H., Boldt, E. A., Holt, S. S., and Serlemitsos, P. J. 1978, *Ap. J.*, **225**, 988.
Pravdo, S. H., White, N. E., Boldt, E. A., Holt, S. S., Serlemitsos, P. J., Swank, J. H., and Szymkowiak, A. E. 1979, *Ap. J.*, **231**, 912.
Rose, L. A., Pravdo, S. H., Kaluzienski, L. J., Marshall, F. E., Holt, S. S., Boldt, E. A., Rothschild, R. E., and Serlemitsos, P. J. 1979, *Ap. J.*, **231**, 919.
Rybicki, G. B., and Lightman, A. P. 1979, *Radiative Processes in Astrophysics* (New York: Wiley-Interscience).
Shakura, N. I., and Sunyaev, R. A. 1973, *Astr. Ap.*, **24**, 337.
Sitenko, A. G. 1967, *Electromagnetic Fluctuations in Plasmas* (London: Academic Press).
Tsuruta, S. 1975, *Ann. NY Acad. Sci.*, **262**, 391.
Ventura, J. 1979, *Phys. Rev. D*, **19**, 1684.
Ventura, J., Nagel, W., and Mészáros, P. 1979, *Ap. J. (Letters)*, **233**, L125.
Voges, W., Pietsch, W., Reppin, C., Trümper, J., Kendziorra, E., and Staubert R. 1982, *Ap. J.*, **263**, 803.
Wang, Y. M., and Frank, J. 1981, *Astr. Ap.*, **93**, 255.
Wasserman, I., and Salpeter, E. E. 1980, *Ap. J.*, **241**, 1107.
White, N. E., Swank, J. H., and Holt, S. S. 1983, *Ap. J.*, **270**, 711.
Yahel, R. Z. 1980, *Astr. Ap.*, **90**, 26.
Zel'dovich, Ya. B., and Shakura, N. I. 1969, *Soviet Astr.—AJ*, **13**, L175.

D. J. GALLOWAY and J. G. KIRK: Max-Planck-Institut für Physik und Astrophysik, Institut für Astrophysik, Karl-Schwarzschild-Str. 1, 8046 Garching bei München, Federal Republic of Germany

A. K. HARDING: Code 665, NASA Goddard Space Flight Center, Greenbelt, MD 20771

P. MÉSZÁROS: Astronomy Department, 506 Davey Lab, Pennsylvania State University, University Park, PA 16802